Electrically pumped semiconductor laser with low spatial coherence and directional emission

Cite as: Appl. Phys. Lett. **115**, 071101 (2019); doi: 10.1063/1.5109234
Submitted: 7 May 2019 · Accepted: 3 July 2019 ·
Published Online: 12 August 2019

View Online Export Citation CrossMark

Kyungduk Kim,[1] Stefan Bittner,[1] Yongquan Zeng,[2] Seng Fatt Liew,[1] Qijie Wang,[2] and Hui Cao[1,a)]

AFFILIATIONS

[1]Department of Applied Physics, Yale University, New Haven, Connecticut 06520, USA
[2]Center for OptoElectronics and Biophotonics, School of Electrical and Electronic Engineering and the Photonics Institute, Nanyang Technological University, 639798 Singapore

[a)]Electronic mail: hui.cao@yale.edu

ABSTRACT

We design and fabricate an on-chip laser source that produces a directional beam with low spatial coherence. The lasing modes are based on the axial orbit in a stable cavity and have good directionality. To reduce the spatial coherence of emission, the number of transverse lasing modes is maximized by fine-tuning the cavity geometry. In a cavity with the size of hundreds of micrometers, 1000 transverse modes lase simultaneously and independently, reducing the speckle contrast to 0.03. Decoherence is reached in a few nanoseconds as a result of frequency detuning of lasing modes. Such rapid decoherence will facilitate applications in ultrafast speckle-free full-field imaging.

The high spatial coherence of conventional lasers can introduce coherent artifacts due to uncontrolled diffraction, reflection, and optical aberration. A common example is the speckle formed by the interference of coherent waves with random phase differences.[1,2] Speckle noise is detrimental to full-field imaging applications such as displays,[3] microscopy, optical coherence tomography, and holography.[4] It also poses a problem for laser-based applications like material processing, photolithography, and optical trapping of particles.

Various approaches to mitigate speckle artifacts have been developed. A traditional method is to average over many independent speckle patterns generated by a moving diffuser,[5,6] colloidal solution,[7] or fast scanning micromirrors.[8] However, the generation of a series of uncorrelated speckle patterns is time-consuming and limited by the mechanical speed. A more efficient approach is to design a multimode laser that generates spatially incoherent emission, thus directly suppressing speckle formation.[9] Low spatial coherence necessitates lasing in numerous distinct spatial modes with independent oscillation phases. For example, a degenerate cavity[10–12] allows a large number of transverse modes to lase, but the setup is bulky and hard to align. Complex lasers with a compact size such as random lasers[13–16] have low spatial coherence and high photon degeneracy but are mostly optically pumped. For speckle-free imaging applications, wave-chaotic semiconductor microlasers[17] have the advantages of electrical pumping and high internal quantum efficiency. However, disordered or wave-chaotic cavity lasers typically have no preferential emission direction, and the poor collection efficiency greatly reduces their external quantum efficiency. Our goal is to create an electrically pumped multimode semiconductor microlaser without disordered or wave-chaotic cavities to combine low spatial coherence and directional emission.

Moreover, the speed of speckle suppression is crucial for imaging applications. For instance, time-resolved optical imaging to observe fast dynamics requires speckle-free image acquisition with a short integration time, and so the oscillation phases of different spatial lasing modes must completely decorrelate during the integration time to attain decoherence. The finite linewidth $\Delta\nu$ of individual lasing modes leads to their decoherence on a time scale of $1/\Delta\nu$. The frequency difference between different lasing modes can lead to even faster decoherence. For example, the emission from many random lasing modes with distinct frequencies exhibits low spatial coherence already within ten nanoseconds.[18] The decoherence time was measured for a solid-state degenerate cavity laser.[19] The intensity contrast of the laser speckle is reduced by the dephasing between different longitudinal mode groups in tens of nanoseconds, but complete decoherence requires a few microseconds due to the small frequency spacing between transverse modes. We aim to further shorten the decoherence time by utilizing the larger mode spacings in a semiconductor microlaser.

Here, we design an electrically pumped chip-scale semiconductor laser with spatially incoherent and directional emission. The emission from conventional broad-area semiconductor lasers with flat end mirrors exhibits a good directionality. However, lasing occurs only in a few transverse modes since the high-order transverse modes have large divergence angles and hence experience severe losses.[20,21] To lower the spatial coherence, we need to increase the number of transverse lasing modes. With curved end mirrors, the losses of high-order transverse modes can be reduced. We consider two-dimensional (2D) symmetric cavities with two circular concave mirrors with radius of curvature R_c as shown in Fig. 1(a). The mirrors are separated by the cavity length L. The geometry of the cavity is determined by the parameter $g = 1 - L/R_c$, which is known as the cavity stability parameter. If R_c is larger than $L/2$ or g is within the range $(-1, 1)$, the cavity is called stable in the sense that rays starting near the cavity axis stay close to it and will remain inside the cavity.[22] In the paraxial limit, the resonances in the stable cavity are described by Hermite-Gaussian modes, which have different transverse profiles depending on the transverse mode number m. Figure 1(b) shows the spatial intensity profile of a high-order transverse mode with $m = 10$.

Reducing the speckle contrast $C = 1/\sqrt{M}$ to below the level of human perception $\simeq 0.03$[23,24] requires $M \sim 1000$ transverse modes to lase simultaneously and independently. Previous designs of stable cavity semiconductor lasers with curved facets[25–27] exhibited less than 10 transverse lasing modes. The challenge is to increase the number of transverse lasing modes by two orders of magnitude. To accommodate higher order transverse modes, we increase the cavity width W. For directional emission, all lasing modes must be based on the axial orbit, which is formed by a ray traveling back and forth along the cavity axis between the two mirrors. However, modes based on nonaxial orbits like those in Fig. 1(c) can appear in wide cavities, yielding nondirectional emission. We eliminate the reflecting surfaces at the lateral sides [black dashed lines in Fig. 1(c)] to suppress the nonaxial modes based on the periodic orbits with bounces from the sidewalls, such as the diamond orbit.[26,27] In addition, we set $W = L/\sqrt{2}$ to avoid the rectangle orbits in the stable cavity. A schematic of our design is shown in Fig. 1(d).

To maximize the number of transverse modes with similarly high Q factors, we optimize the cavity shape by fine tuning R_c while keeping L and W fixed. We numerically calculate the passive cavity modes using the finite element method (COMSOL). A 2D cavity with $L = 20\ \mu$m is simulated. The refractive index of the cavity $n = 3.37$ corresponds to the effective refractive index of the vertically guided mode in the GaAs wafer used in the experiment. Transverse-electric (TE) polarization (electric field parallel to the cavity plane) is considered since GaAs quantum wells have higher gain for this polarization and the lasing modes are TE polarized.

Degenerate cavities with conventional mirrors can support transverse modes with nearly degenerate Q-factors thanks to their self-imaging property.[28,29] As an example of a degenerate cavity, we consider the confocal geometry ($g = 0$). For the on-chip design with dielectric interfaces as mirrors, however, the Q-factor decreases significantly as the transverse mode number m increases as shown in Fig. 2(a). Figure 2(b) shows a typical mode laterally confined to the cavity axis, resulting in negligible diffraction loss. We calculate its Husimi projection[30] from the overlap of its spatial field distribution with a minimal-uncertainty wave packet impinging onto the cavity boundary. It visualizes the angle of incidence χ of wave components at different positions s of the cavity boundary. The high-intensity spots in the Husimi map indicate that the dominant wave components have a nonzero angle of incidence onto the cavity mirrors. As m increases, wave components with increasingly higher incident angles appear. Thus, high-order transverse modes in the confocal cavity experience higher loss since the reflectivity at a dielectric-air interface decreases with increasing χ for TE-polarized light, making the confocal cavity unsuitable for multimode lasing.

To solve this problem, we consider the concentric cavity ($g = -1$), which does not have frequency degeneracy of its resonances.

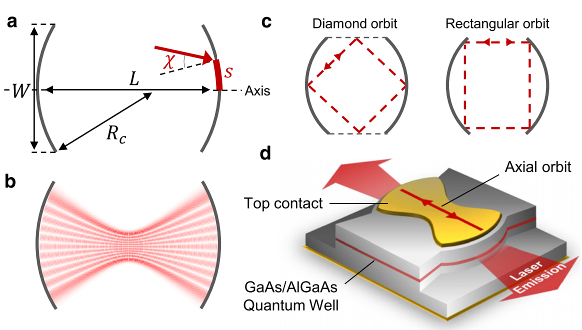

FIG. 1. Schematic of the on-chip stable cavity laser. (a) 2D symmetric stable cavity defined by two concave circular mirrors with radius of curvature R_c and distance L. The cavity width W is the distance between two extremities of a curved mirror. Rays impinging on the cavity boundary are described by coordinates (s, χ), where s is the coordinate along the curved boundary and χ is the angle of incidence with respect to the surface normal. (b) The spatial intensity profile of a high-order transverse mode in a stable cavity. (c) Nonaxial orbits that lead to nondirectional emission. (d) Three-dimensional sketch of the on-chip stable cavity with directional emission. The lasing modes are based on the axial orbit and thus have directional emission. The shape of the top metal contact matches the spatial profile of high-order transverse modes to ensure their spatial overlap with gain.

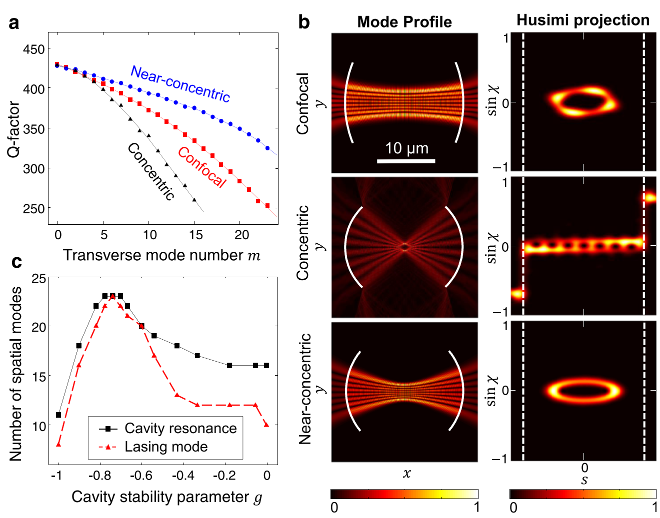

FIG. 2. Fine tuning of the cavity geometry to maximize the number of transverse modes. (a) Dependence of quality factor Q on transverse mode number m for the optimized near-concentric ($g = -0.74$), confocal ($g = 0$), and concentric ($g = -1$) cavities. (b) Calculated spatial distributions of field amplitude (left) and corresponding Husimi projections (right) for high-order transverse modes ($m = 7$) in confocal, concentric, and near-concentric ($g = -0.74$) cavities. White solid lines in the left column represent the curved cavity facets, and while dashed lines in the right column mark the endpoints of the facets. (c) Calculated number of high-Q resonances (black squares) and the number of lasing modes (red triangles) that are based on axial orbit and exhibit distinct transverse profiles as a function of cavity stability parameter g.

Since the concentric mirrors are part of a circle, any ray passing through the cavity center hits the boundaries perpendicularly. Indeed, the Husimi projection in Fig. 2(b) is strongly localized at $\chi = 0$, and thus, the angle-dependent reflectance is an insignificant loss mechanism. However, as the mode profile exhibits a large divergence, light leaks out via diffraction from the endpoints of the facets. These losses are evident in the Husimi projection from the high-intensity spots just outside the cavity facet. Since the higher order transverse modes experience stronger diffraction loss, the Q-factor decreases even more quickly with m than for the confocal case as seen in Fig. 2(a).

We gradually vary g from -1 to 0 in search for the optimal geometry that supports the largest number of high-Q transverse modes. Figure 2(c) shows the number of transverse modes, which are based on the axial orbit and have Q-factors exceeding 0.8 times the maximal Q-factor, as a function of g. The optimal geometry $g = -0.74$ is near concentric. A slight deviation from the concentric shape makes the mode profiles laterally localized to the cavity axis [see Fig. 2(b)]. Moreover, the Husimi projection shows high-intensity spots centered at $\chi = 0$, which indicates that most wave components have almost normal incidence on the cavity facet. Therefore, the near-concentric geometry minimizes both losses from angle-dependent reflectance and diffraction, resulting in the slowest decrease in Q with m. As the number of transverse modes scales linearly with the width W of the cavity when keeping the ratio W/L fixed, we can apply this optimization result to the larger cavities used in experiments (see the supplementary material).

The above optimization is based on the cavity resonances in the absence of gain. Gain competition can limit the number of lasing modes additionally. In order to quantify the effect of gain competition, we calculate the number of lasing modes at steady state[31] (see the supplementary material). The red curve in Fig. 2(c) represents the number of different transverse lasing modes at a pump level of two times above the lasing threshold. In the confocal cavity, the number of lasing modes based on the axial orbit is notably smaller than the number of high-Q passive modes due to the existence of nonaxial modes with higher Q which lase first and saturate the gain for the axial modes (see the supplementary material). For the optimized near-concentric cavity, most of the passive transverse modes with high Q can lase, indicating that gain competition is insignificant.

The experimental results for the on-chip stable cavity lasers are presented in Fig. 3. The cavities are fabricated by photolithography followed by reactive ion etching from a commercial GaAs/AlGaAs quantum well epiwafer. To ensure the spatial overlap of high-Q transverse modes with the quantum well gain, the top metal contact for current injection is shaped to match the spatial profile of the highest-order transverse lasing modes. The scanning electron microscopy (SEM) images in Fig. 3(a) show that the etched facets, which serve as curved end mirrors, are smooth and vertical. The fabricated sample is mounted on a copper block, and a tungsten needle is placed on the top gold contact for current injection. Lasing is observed at room temperature with electrical pumping for all the tested cavities with different sizes and shapes. To reduce heating, the current pulses are 2 μs-long with a 10 Hz repetition rate. The emission is collected by an objective lens (NA = 0.4) and coupled into a spectrometer. The inset of Fig. 3(b) shows the emission spectra from an optimized near-concentric cavity ($g = -0.74$) at different pump currents. A typical spectrum consists of many closely spaced narrow peaks, indicating simultaneous lasing of many modes. More lasing peaks appear at higher pump currents, and they merge to a smooth, broad spectrum. The curve of emission power vs pump current for an $L = 400$ μm-long cavity in Fig. 3(b) shows a lasing threshold of 360 mA, above which the emission power increases much more rapidly with the pump current. The total emission power reaches 350 mW at a pump current of 800 mA, and the differential quantum efficiency is 0.8 W/A. The threshold current density is inversely proportional to the cavity length L (not shown) as expected since the Q-factors increase with L linearly.[22] There is no significant difference between the lasing thresholds for cavities with the same L but different g.

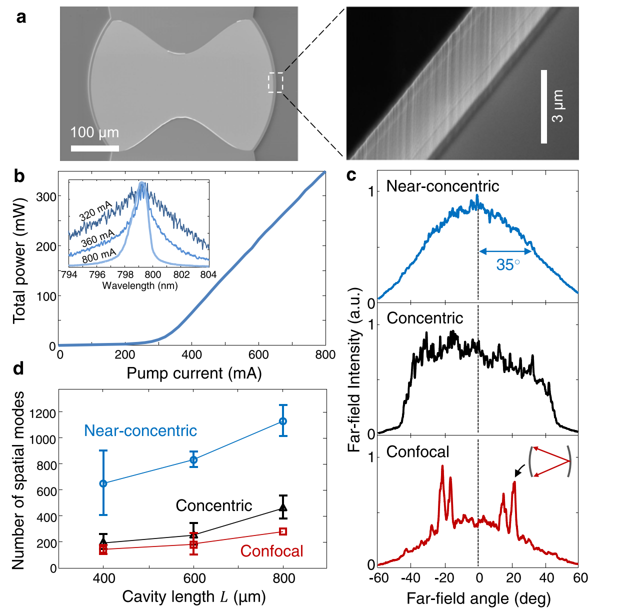

FIG. 3. Lasing characteristics of the on-chip stable cavities. (a) SEM images of a fabricated near-concentric ($g = -0.74$) cavity of length $L = 400$ μm. The etched facet is vertical and smooth. (b) Total emission power vs pump current of a near-concentric cavity with $L = 400$ μm. Inset: normalized emission spectra at different pump currents. (c) Far-field intensity patterns of laser emission from three cavities with $g = -0.74$, -1, and 0. The V-shaped orbit, which contributes to the sharp peaks in the far-field pattern of the confocal cavity, is drawn in the inset. (d) The number of transverse lasing modes in near-concentric ($g = -0.74$), concentric ($g = -1$), and confocal ($g = 0$) cavities with different lengths L. The error bars indicate the variation between different cavities of the same g and L.

To investigate the emission directionality, we measure the far-field emission patterns at a pump current two times above the lasing threshold. Figure 3(c) shows the far-field patterns for three cavity shapes. The far-field emission was measured at a distance $D = 6$ cm from the cavity facet. For a near-concentric cavity ($g = -0.74$), a directional output beam with a divergence angle (half width at half maximum) of 35° is observed. The concentric cavity ($g = -1$) shows a flat-top far-field pattern with sharp edges. This pattern is attributed to the broad angular divergence of modes in the concentric cavity. In contrast, the far-field pattern of the confocal cavity features sharp peaks on top of a broad background. The sharp peaks originate from lasing modes based on a V-shaped, nonaxial orbit (see the inset and supplementary material).

We characterize the spatial coherence of the laser emission from the cavities of different shapes. The emission is coherent in the direction normal to the wafer since the sample has only one index-guided mode in the vertical direction. To measure the coherence of emission in the horizontal direction (parallel to the wafer), we create speckle patterns with a line diffuser that scatters light only in the horizontal direction. A CCD camera records the far-field speckle intensity pattern generated by laser emission from a single 2 μs-long pump pulse [see Fig. 4(a)]. In order to quantify the spatial coherence, we calculate the speckle contrast defined as $C = \sigma_I / \langle I \rangle$, where σ_I and $\langle I \rangle$ are the standard deviation and mean of the speckle intensity, respectively. $M = 1/C^2$ gives the effective number of distinct transverse lasing modes.[1] Figure 3(d) shows the values of M for cavities with different g and L, measured at two times the lasing threshold. The number of transverse lasing modes is the largest for the near-concentric cavity ($g = -0.74$). With the ratio W/L fixed, the number of transverse modes increases with L since a wider cavity supports more transverse modes. For the $L = 800\ \mu$m near-concentric cavity ($g = -0.74$), about 1000 different transverse modes lase, and their combined emission reduces the speckle contrast to about 0.03.

To examine the applicability of the optimized laser for ultrafast speckle-free imaging, we determine how fast decoherence of the emission occurs. We use a streak camera to measure the time-resolved speckle patterns with a temporal resolution of about 60 ps in a setup sketched in Fig. 4(a). Figure 4(b) shows the spatiotemporal evolution of the measured far-field speckle pattern of a near-concentric cavity laser ($g = -0.74$). The magnification in Fig. 4(c) reveals rapid spatial and temporal variations of the intensity pattern. To quantify the coherence time of the emission, we calculate the contrast of speckle patterns as a function of the integration time. As shown in Fig. 4(d), for a short integration time of $t_{\mathrm{int}} = 0.2$ ns, the speckle has a notable

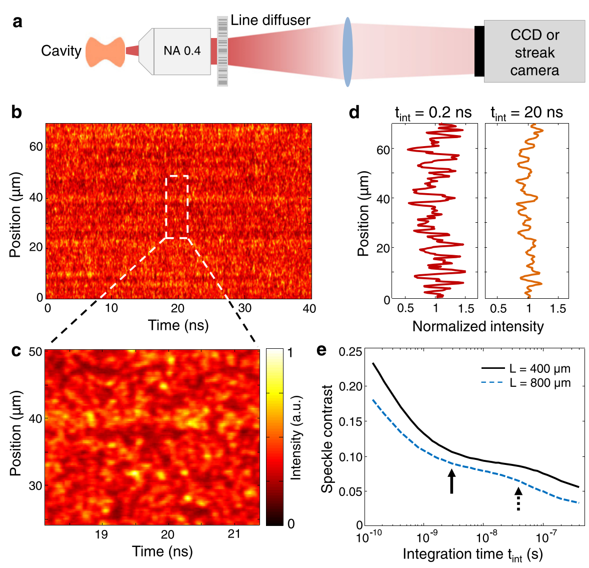

FIG. 4. Decoherence time for a near-concentric cavity laser. (a) Schematic of the setup that measures speckle patterns with a CCD or streak camera. (b) The spatiotemporal profile of the far-field speckle pattern from a laser with $g = -0.74$ and $L = 400\ \mu$m. (c) Magnification of the speckle pattern revealing fast temporal evolution of the speckle grains. (d) Time-integrated speckle patterns for integration times of 0.2 ns and 20 ns, exhibiting an intensity contrast of $C = 0.21$ and 0.098, respectively. (e) Dependence of speckle contrast on the integration time t_{int}, featuring two kinks at the integration times of a few nanoseconds (solid arrow) and several tens of nanoseconds (dotted arrow).

contrast of $\sim$0.2. As the integration time increases, the speckle contrast drops quickly. Figure 4(e) summarizes the reduction of the speckle contrast for t_{int} from 100 ps to 500 ns. The $L = 800\ \mu$m-long cavity laser features lower speckle contrast than the $L = 400\ \mu$m-long cavity laser for all integration times. After a rapid drop, the contrast starts to saturate, exhibiting a kink at a few nanoseconds (indicated by the solid arrow). A second kink (indicated by a dotted arrow) follows at several tens of nanoseconds after which the speckle contrast further declines.

The time scale of the speckle contrast reduction is related to the frequency differences of lasing modes when their linewidths are smaller than their frequency spacings. When the integration time t_{int} is shorter than the inverse frequency spacing of two modes, their temporal beating results in a visible interference pattern that oscillates in time. For an integration time longer than their beating period, the time-varying interference pattern is averaged out, and hence, the intensity contrast of the speckle pattern created by these two modes is reduced. With increasing integration time, more and more lasing modes become incoherent, as their frequency spacings exceed $1/t_{\mathrm{int}}$, and the speckle contrast continues dropping. Once t_{int} is long enough to average out the beating of even the closest pairs of lasing modes, the speckle contrast cannot reduce further. The average frequency spacing between adjacent modes is estimated as several hundred megahertz in our cavities (see the supplementary material), whereas the typical linewidth of semiconductor lasers (10–100 MHz) is smaller than the frequency spacing. Thus, the integration time needed for contrast reduction is determined by the mode spacing and estimated to be a few nanoseconds, which matches the experimental observations. The additional reduction of the speckle contrast at a few ten nanoseconds is attributed to a thermally induced change of lasing modes[32] (see the supplementary material). When the lasing modes change, the output emission patterns change as well and their superposition further reduces the speckle contrast.

In summary, we demonstrate directional emission, low spatial coherence, and ultrashort decoherence time in a compact electrically pumped semiconductor laser. By optimizing the shape of an on-chip near-concentric cavity, we maximize the number of transverse lasing modes and their emission greatly suppresses speckle formation. The frequency detuning of lasing modes accelerates the decoherence of their emission, and low speckle contrast is obtained even with an integration time of a few nanoseconds. Such short decoherence time enables ultrafast speckle-free full-field imaging. Finally, we compare this work to the previous demonstration of spatially incoherent nonmodal emission from a broad-area vertical-cavity surface-emitting laser.[33] By carefully adjusting the pump conditions, the cavity is constantly modified by thermal effects, which disrupts the formation of lasing modes, leading to spatially incoherent emission.[34,35] Our approach does not rely on thermal effects, and the decoherence time is two orders of magnitude shorter. Furthermore, our method does not utilize any transient process, and thus, it is applicable to steady-state lasing. With better thermal management, our laser may operate under constant pumping, emitting a continuous wave of low spatial coherence.

See the supplementary material for additional details of the experiment and numerical simulations.

We thank N. Davidson, R. Chriki, and A. D. Stone for fruitful discussions. This work conducted at Yale University was supported by the Air Force Office of Scientific Research (AFOSR) under Grant No. FA9550-16-1-0416 and by the Office of Naval Research (ONR) with MURI Grant No. N00014-13-1-0649. The work at Nanyang Technological University was financially supported by the Ministry of Education, Singapore grant (Nos. MOE2016-T2-1-128 and MOE2016-T2-2-159) and National Research Foundation, Competitive Research Program (No. NRF-CRP18-2017-02).

REFERENCES

[1] J. W. Goodman, *Speckle Phenomena in Optics: Theory and Applications* (Roberts and Company Publishers, 2007).
[2] J. C. Dainty, *Laser Speckle and Related Phenomena* (Springer Science & Business Media, 2013), Vol. 9.
[3] K. V. Chellappan, E. Erden, and H. Urey, "Laser-based displays: A review," Appl. Opt. **49**, F79–F98 (2010).
[4] V. Bianco, P. Memmolo, M. Leo, S. Montresor, C. Distante, M. Paturzo, P. Picart, B. Javidi, and P. Ferraro, "Strategies for reducing speckle noise in digital holography," Light: Sci. Appl. **7**, 48 (2018).
[5] S. Lowenthal and D. Joyeux, "Speckle removal by a slowly moving diffuser associated with a motionless diffuser," J. Opt. Soc. Am. **61**, 847–851 (1971).
[6] S. Kubota and J. W. Goodman, "Very efficient speckle contrast reduction realized by moving diffuser device," Appl. Opt. **49**, 4385–4391 (2010).
[7] B. Redding, G. Allen, E. R. Dufresne, and H. Cao, "Low-loss high-speed speckle reduction using a colloidal dispersion," Appl. Opt. **52**, 1168–1172 (2013).
[8] M. N. Akram, Z. Tong, G. Ouyang, X. Chen, and V. Kartashov, "Laser speckle reduction due to spatial and angular diversity introduced by fast scanning micromirror," Appl. Opt. **49**, 3297–3304 (2010).
[9] H. Cao, R. Chriki, S. Bittner, A. A. Friesem, and N. Davidson, "Complex lasers with controllable coherence," Nat. Rev. Phys. **1**, 156–168 (2019).
[10] M. Nixon, B. Redding, A. A. Friesem, H. Cao, and N. Davidson, "Efficient method for controlling the spatial coherence of a laser," Opt. Lett. **38**, 3858–3861 (2013).
[11] R. Chriki, M. Nixon, V. Pal, C. Tradonsky, G. Barach, A. A. Friesem, and N. Davidson, "Manipulating the spatial coherence of a laser source," Opt. Express **23**, 12989–12997 (2015).
[12] S. Knitter, C. Liu, B. Redding, M. K. Khokha, M. A. Choma, and H. Cao, "Coherence switching of a degenerate VECSEL for multimodality imaging," Optica **3**, 403–406 (2016).
[13] C. Gouedard, D. Husson, C. Sauteret, F. Auzel, and A. Migus, "Generation of spatially incoherent short pulses in laser-pumped neodymium stoichiometric crystals and powders," J. Opt. Soc. Am. B **10**, 2358–2363 (1993).
[14] B. Redding, M. A. Choma, and H. Cao, "Spatial coherence of random laser emission," Opt. Lett. **36**, 3404–3406 (2011).
[15] B. Redding, M. A. Choma, and H. Cao, "Speckle-free laser imaging using random laser illumination," Nat. Photonics **6**, 355 (2012).
[16] B. H. Hokr, M. S. Schmidt, J. N. Bixler, P. N. Dyer, G. D. Noojin, B. Redding, R. J. Thomas, B. A. Rockwell, H. Cao, V. V. Yakovlev *et al.*, "A narrow-band speckle-free light source via random Raman lasing," J. Mod. Opt. **63**, 46–49 (2016).
[17] B. Redding, A. Cerjan, X. Huang, M. L. Lee, A. D. Stone, M. A. Choma, and H. Cao, "Low spatial coherence electrically pumped semiconductor laser for speckle-free full-field imaging," Proc. Natl. Acad. Sci. U. S. A. **112**, 1304–1309 (2015).
[18] A. Mermillod-Blondin, H. Mentzel, and A. Rosenfeld, "Time-resolved microscopy with random lasers," Opt. Lett. **38**, 4112–4115 (2013).
[19] R. Chriki, S. Mahler, C. Tradonsky, V. Pal, A. A. Friesem, and N. Davidson, "Spatiotemporal supermodes: Rapid reduction of spatial coherence in highly multimode lasers," Phys. Rev. A **98**, 023812 (2018).
[20] R. J. Lang, A. G. Larsson, and J. G. Cody, "Lateral modes of broad area semiconductor lasers: Theory and experiment," IEEE J. Quantum Electron. **27**, 312 (1991).
[21] S. Hartmann and W. Elsäßer, "A novel semiconductor-based, fully incoherent amplified spontaneous emission light source for ghost imaging," Sci. Rep. **7**, 41866 (2017).
[22] A. E. Siegman, *Lasers* (University Science Books, 1986).
[23] S. Roelandt, Y. Meuret, A. Jacobs, K. Willaert, P. Janssens, H. Thienpont, and G. Verschaffelt, "Human speckle perception threshold for still images from a laser projection system," Opt. Express **22**, 23965–23979 (2014).
[24] G. A. Geri and L. A. Williams, "Perceptual assessment of laser-speckle contrast," J. Soc. Inf. Disp. **20**, 22–27 (2012).
[25] S. A. Biellak, Y. Sun, S. S. Wong, and A. E. Siegman, "Lateral mode behavior of reactive-ion-etched stable-resonator semiconductor lasers," J. Appl. Phys. **78**, 4294–4296 (1995).
[26] T. Fukushima, T. Harayama, P. Davis, P. O. Vaccaro, T. Nishimura, and T. Aida, "Ring and axis mode lasing in quasi-stadium laser diodes with concentric end mirrors," Opt. Lett. **27**, 1430–1432 (2002).
[27] T. Fukushima, S. Sunada, T. Harayama, K. Sakaguchi, and Y. Tokuda, "Lowest-order axial and ring mode lasing in confocal quasi-stadium laser diodes," Appl. Opt. **51**, 2515–2520 (2012).
[28] J. Arnaud, "Degenerate optical cavities," Appl. Opt. **8**, 189–196 (1969).
[29] S. Gigan, L. Lopez, N. Treps, A. Maître, and C. Fabre, "Image transmission through a stable paraxial cavity," Phys. Rev. A **72**, 023804 (2005).
[30] M. Hentschel, H. Schomerus, and R. Schubert, "Husimi functions at dielectric interfaces: Inside-outside duality for optical systems and beyond," Europhys. Lett. **62**, 636 (2003).
[31] A. Cerjan, B. Redding, L. Ge, S. F. Liew, H. Cao, and A. D. Stone, "Controlling mode competition by tailoring the spatial pump distribution in a laser: A resonance-based approach," Opt. Express **24**, 26006–26015 (2016).
[32] S. Bittner, S. Guazzotti, Y. Zeng, X. Hu, H. Yilmaz, K. Kim, S. Oh, Q. Wang, O. Hess, and H. Cao, "Suppressing spatiotemporal lasing instabilities with wave-chaotic microcavities," Science **361**, 1225–1231 (2018).
[33] M. Peeters, G. Verschaffelt, H. Thienpont, S. K. Mandre, I. Fischer, and M. Grabherr, "Spatial decoherence of pulsed broad-area vertical-cavity surface-emitting lasers," Opt. Express **13**, 9337–9345 (2005).
[34] S. K. Mandre, W. Elsäßer, I. Fischer, M. Peeters, and G. Verschaffelt, "Evolution from modal to spatially incoherent emission of a broad-area VCSEL," Opt. Express **16**, 4452–4464 (2008).
[35] G. Craggs, G. Verschaffelt, S. K. Mandre, H. Thienpont, and I. Fischer, "Thermally controlled onset of spatially incoherent emission in a broad-area vertical-cavity surface-emitting laser," IEEE J. Sel. Top. Quantum Electron. **15**, 555–562 (2009).